Magnesium Oxide Nanoparticles: Potent Antibacterial and Antioxidant Nanostructures

Baitha, R. R.[1], Srivastava, M.[1] and Ahmad, S.[1]

[1]University Department of Botany, Jai Prakash University, Chhapara, Bihar, India

Corresponding Author:
Prof (Dr.) Md. Sarfaraz Ahmad
University Department of Botany
Jai Prakash University
Chhapara, Bihar, India
mdsarfarazahmad786@gmail.com

ABSTRACT:

Bacterial-borne infections pose a serious threat in tropical and subtropical regions, and with rising resistance issues, effective control has become a pressing concern. This study explores the synthesis of magnesium oxide (MgO) nanoparticles using four innovative methods: green synthesis, microwave-assisted synthesis, sol-gel and hydrothermal techniques. The resulting MgO nanoparticles were characterized via FT-IR (Fourier Transform Infrared Spectroscopy), XRD (X-ray Diffraction), SEM (Scanning Electron Microscopy), and EDAX (Energy-Dispersive X-ray Analysis). FT-IR confirmed the presence of functional groups, while XRD and HRSEM unveiled structural and morphological details. EDAX validated the elemental composition, highlighting Mg and O.

Antibacterial efficacy was tested against Gram-positive bacteria (*Enterococcus faecalis*) and. Among the three synthesis methods, hydrothermally synthesized MgO nanoparticles at 50 mg/mL exhibited the highest activity—producing zones of inhibition (ZOI) of 7 mm for *E. faecalis* showed the greatest sensitivity, with a 9 mm ZOI using sol-gel-produced MgO.

Further, antioxidant activity was tested against synthesized MgO nanostructures proved most effective, achieving a great Antioxidant (SOD) of unit 15.558 unit/mg , while green-synthesized variants showed the lowest (11.493 unit/mg). These findings position MgO nanostructures as promising dual-function agents for both antibacterial therapy and Antioxidant properties.

Keywords: Magnesium nanoparticles, Antibacterial activity and Anti-oxidant activity.

INTRODUCTION

Vector-borne diseases such as cholera, gastro intestinal disease, fever, and many continue to pose major global health challenges[1]. Bacteria like *E. ficalis* are key contributors to the transmission of these diseases. *E. ficalis* alone puts over 1.23 billion people at risk, with an estimated 2.42 billion infections reported annually across 128 countries—mostly within tropical and subtropical regions[2]. In India, more than 31,000 cases were reported in 2017.

Due to bateria's restricted mobility, bactericidal strategies offer advantages such as better bio-efficacy, targeted application, and environmental safety. Nanotechnology has emerged as a promising approach to develop eco-friendly and efficient bactericide[2]. Nanoparticles (NPs) can be synthesized using biological, chemical, or physical methods. The biological route utilizes plant extracts (green synthesis), while the chemical method uses chemical reagents, and the physical method relies on external energy sources like radiation[4].

Among various nanomaterials, metal and metal oxide nanoparticles—like those of Au, Ag, ZnO, MgO, TiO_2, CuO, and CeO_2—have demonstrated potent larvicidal properties[4]. Magnesium oxide nanoparticles (MgO NPs) stand out for their low toxicity, cost-effectiveness, and wide availability. They have gained recognition for applications in nanomedicine and environmental protection[3].

This study focuses on the synthesis of MgO nanostructures using four different methods:

1. **Green synthesis** – eco-friendly and low in chemical usage.
2. **Microwave irradiation** – rapid, efficient heating with better control.
3. **Sol–gel method** – economical and operable at low temperatures.

These synthesized MgO nanostructures were characterized and evaluated for both antibacterial and antioxidant activity against mosquito species, indicating their potential as effective and sustainable vector control agents[5].

MATERIALS AND METHODS

Chemicals and Plant Material

Magnesium nitrate hexahydrate [$Mg(NO_3)_2 \cdot 6H_2O$] and sodium hydroxide (NaOH) were procured from Merck. All other reagents used were of analytical grade[4]. *Psidium guajava* leaves were collected from Lucknow, India.

Synthesis of MgO Nanoparticles (MgO NPs)

1. Green Synthesis (G-MgO)

Fresh *P. guajava* leaves were washed thoroughly, shade-dried for 5–6 days, and ground into a fine powder[6]. Ten grams of this powder was mixed with water, heated at 50 °C, and stirred for 30 minutes. After cooling, the solution was filtered and stored at 4 °C.

A solution of 0.1 mM magnesium nitrate hexahydrate (1.8 g in 100 mL deionized water) was stirred for 15 minutes. To this, 15 mL of the prepared *P[1]. guajava* extract was added and stirred for 3 hours, resulting in a brownish-yellow mixture—indicative of magnesium hydroxide (MgH) NP formation. The suspension was washed with water and ethanol, centrifuged at 4000 rpm for 10 minutes, and calcined at 400 °C for 4 hours to obtain MgO NPs. The plant extract acted as both reducing and capping agent, eliminating the need for additional chemicals like NaOH[5].

2. Microwave-Assisted Synthesis (M-MgO)

A 0.1 mM solution of magnesium nitrate hexahydrate was prepared (1.8 g in 100 mL deionized water) and stirred for 30 minutes[7]. NaOH (0.1 M) was added, forming a white suspension indicative of MgH NP formation. This mixture was irradiated in a microwave furnace for 15 minutes. The product was washed, centrifuged (4000 rpm, 10 min), and calcined at 400 °C for 4 hours to yield MgO NPs[4].

3. Sol–Gel Method (SG-MgO)

Magnesium nitrate hexahydrate (0.1 mM, 1.8 g) was dissolved in 100 mL deionized water, followed by the addition of 0.1 M NaOH, resulting in the formation of a white suspension (MgH NPs)[6]. The solution was stirred for 6 hours, washed with water and ethanol until neutral pH was achieved, centrifuged at 4000 rpm for 10 minutes, and calcined at 400 °C for 4 hours[9].

Characterization Techniques

- **FT-IR Spectroscopy** (PerkinElmer) was used to identify functional groups within the range of 400–4000 cm^{-1}.
- **XRD Analysis** (Bruker D8 Advance, CuKα radiation, $\lambda = 1.5406$ Å) was performed to determine crystalline structure.
- **HR-SEM Imaging** (Thermo Scientific Apreo S) was used to study nanoparticle surface morphology.

Antibacterial Assay

The antibacterial activity of synthesized MgO NPs (G-MgO, M-MgO, SG-MgO) was tested using the **well diffusion method**[8] against *E. ficalis*.

Table 1 Bacterial Strains Used for Antibacterial Analysis Activity

S. No	Type	Bacteria	Culture Collection
1	Gram Positive	*Enterococcus faecalis*	ATCC 9027

Cultures were grown in Mueller–Hinton broth at 35 °C and plated using sterile swabs. Wells (6 mm diameter) were filled with different concentrations of MgO NPs (10, 20, 30, and 50 mg/mL) and ampicillin as control, then incubated at 35 °C for 24 hours. The **zone of inhibition (ZOI)** was measured to assess activity[10].

Anti-oxidant Activity

SOD

A 50 mg sample of the extracted material was taken and thoroughly homogenized in 5 mL of an extraction buffer. The buffer consisted of 150 mM sodium phosphate, adjusted to a pH of 7.0 to maintain the stability of the target compounds during the extraction process[11]. This homogenization step ensured the efficient release of soluble biomolecules from the plant material, facilitating the subsequent analysis of biochemical constituents. The use of sodium phosphate buffer at this specific concentration and pH provided an optimal environment for preserving the integrity of the metabolites while minimizing enzymatic degradation[12].

Catalase

Catalase (CAT) activity was determined using the method outlined by Aebi (1984), which is a widely accepted protocol for assessing catalase activity based on the decomposition of hydrogen peroxide (H_2O_2)[8]. The CAT assay mixture was prepared with a total volume of 3 mL, consisting of the following components: 0.05 mL of the sample extract, 1.5 mL of phosphate buffer (100 mM, pH 7.0) to maintain a stable pH environment, 0.5 mL of hydrogen peroxide (H_2O_2) as the substrate, and 0.95 mL of distilled water to adjust the final volume[13]. **Dose–Response and Statistical Analysis**

Dose-response bioassays were conducted at the same concentration range (7.5–120 ppm). Mortality rates were averaged across five replicates[14]. **Probit analysis** using **SPSS v16.0** was employed to determine **LC_{50} and LC_{90} values**, with results expressed as mean ± standard deviation (n = 3)[14].

Total Phenolic Content

Sample extracted (50 mg), homogenized in a 5 mL extraction buffer comprising 150 mM sodium phosphate buffer at pH 7.

RESULTS AND DISCUSSION

Magnesium oxide (MgO) nanostructures were synthesized through four different approaches: green synthesis, microwave-assisted synthesis, sol–gel technique, and hydrothermal method. Fourier-transform infrared (FT-IR) spectroscopy was employed to identify the functional groups and biomolecules responsible for the capping and stabilization of the synthesized MgO nanoparticles (NPs)[14].

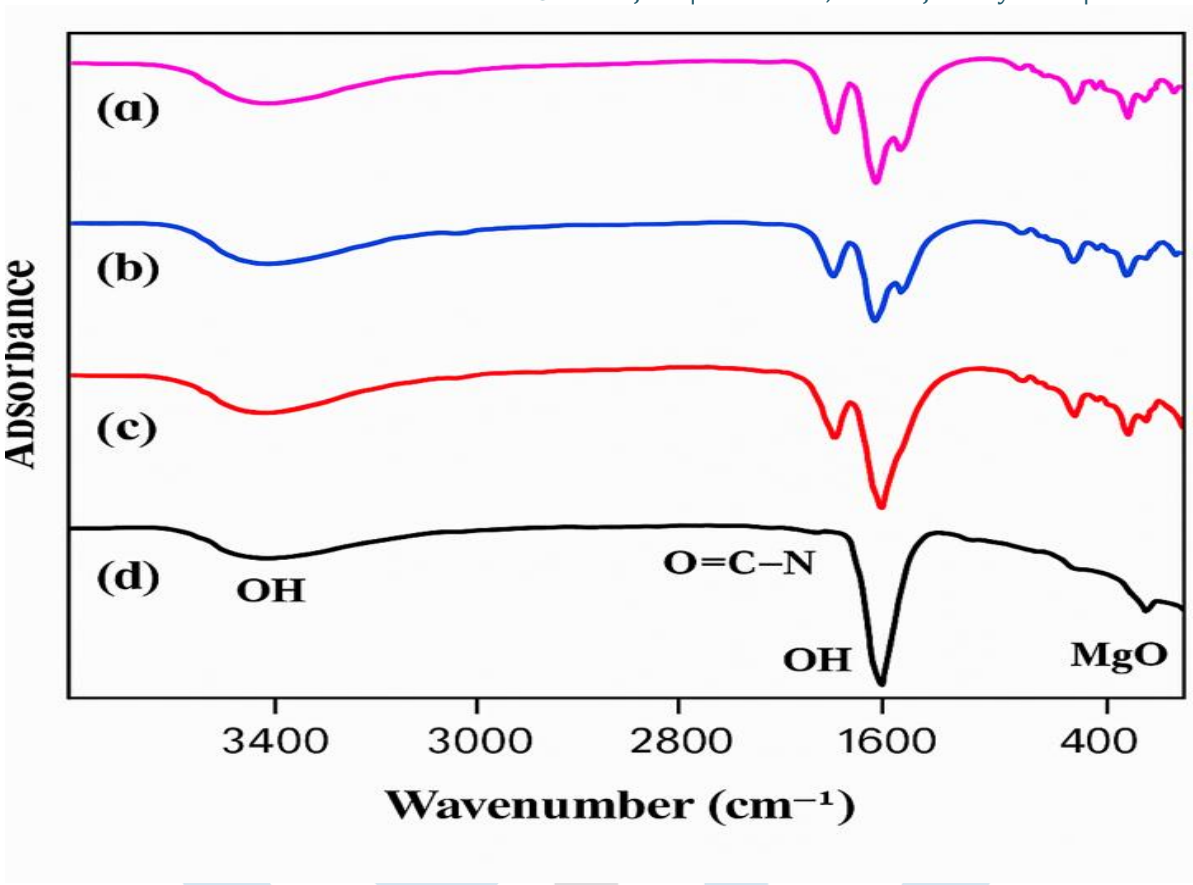

Figure 1. FT-IR image of (bottom to top) green (a), microwave (b), sol−gel (c), and hydrothermal methods (d) of preparation of MgO nanostructures

The FT-IR spectra of the synthesized MgO NPs are illustrated in Figure 1. A prominent broad absorption band around 3420 cm^{-1} is evident in all spectra, which corresponds to the antisymmetric stretching vibrations of hydroxyl (−OH) groups[15]. In particular, the FT-IR spectrum of green-synthesized MgO NPs (Figure 2a) exhibits this broad peak, indicating the presence of polyphenolic compounds derived from *Psidium guajava* leaf extract, which served as a natural reducing and stabilizing agent during synthesis[16].

Similar broad peaks at 3420 cm^{-1} are observed in the spectra of MgO NPs synthesized via microwave (Figure 1b), sol–gel (Figure 1c), and hydrothermal (Figure 1d) methods[14]. These peaks can also be attributed to −OH functional groups, which play a crucial role in the conversion of magnesium precursors into MgO nanoparticles, along with contributions from N−H bending vibrations associated with amine bonds[17].

A medium-intensity peak around 1630 cm^{-1}, observed across all spectra, is ascribed to the bending mode of primary amine (N−H), potentially overlapped with signals from amide or carboxylate salt groups[13]. Additionally, the band at 1647 cm^{-1} is indicative of the presence of amide functional groups.

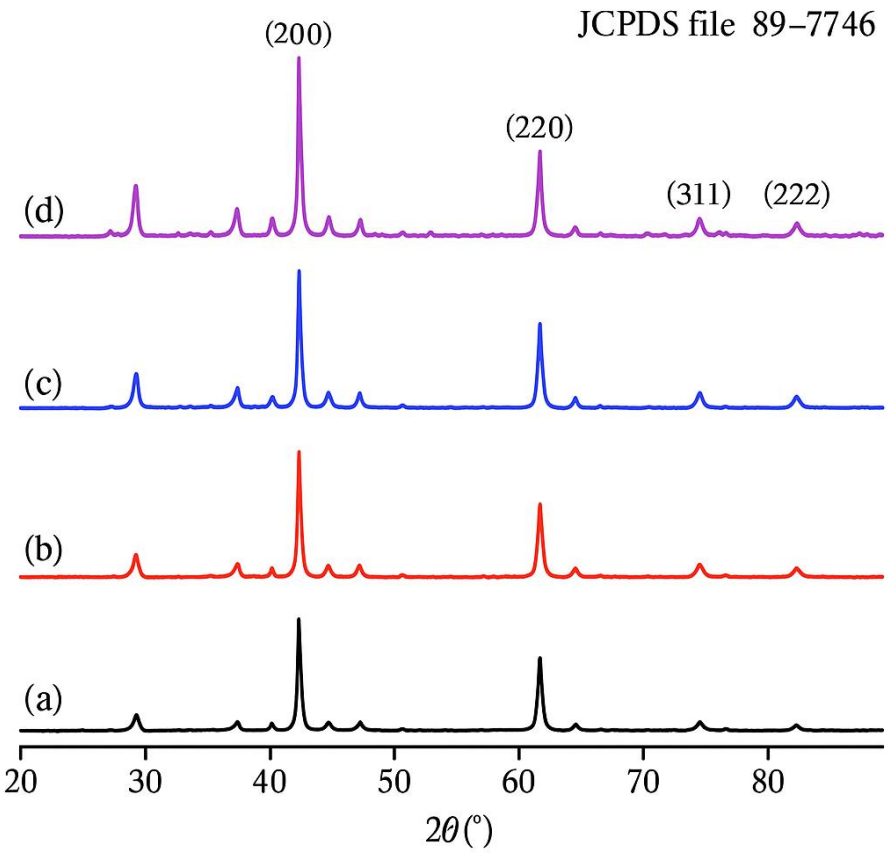

Figure 2. X-ray powder diffraction pattern of (bottom to top) green (a), microwave (b), sol−gel (c), and hydrothermal (d) methods of preparation of MgO nanostructures.

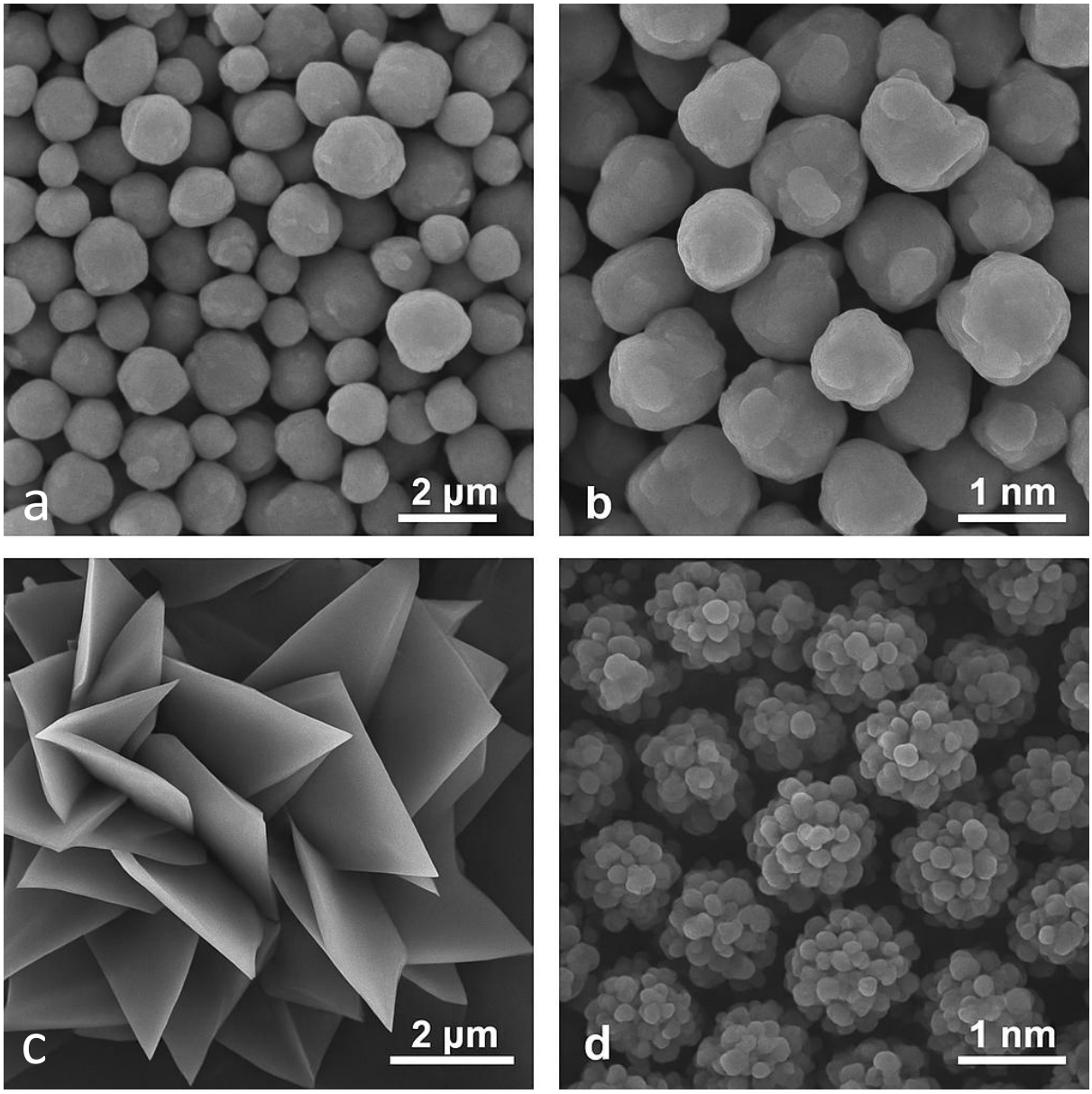

Figure 3. SEM micrographs of (top to bottom) green (a), microwave (b), sol−gel (c), and hydrothermal (d) methods of preparation of MgO nanostructures.

A peak observed at 1484 cm^{-1} corresponds to the vibrational mode of the carbonate ion (C−O). Peaks at 1420 and 1413 cm^{-1} indicate the presence of hydroxyl (OH) groups within the compound. The most intense band (M), appearing at 1351 cm^{-1}, is attributed to the bending vibrations of C−H bonds in aliphatic groups. The peaks in the range of 400–700 cm^{-1} confirm the presence of nanoscale MgO. The FT-IR spectra collectively indicate the purity of the synthesized nanoparticles (NPs) and validate the presence of Mg−O bonds at the nanoscale.

The crystalline structure of MgO nanoparticles synthesized by various methods was examined through X-ray diffraction (XRD) analysis. The XRD spectra (Figure 3) revealed prominent peaks at 2θ values of 42.68°, 62.4°, 74.28°, and 78.62°, which correspond to the (200), (220), (311), and (222) planes, respectively. These diffraction peaks closely match the standard MgO crystallographic data from the JCPDS (file no. 89-7746). Peaks at 2θ values of 29.81°, 75.08°, and 78.64° indicate the presence of $Mg(OH)_2$ in some samples. The average crystallite sizes, calculated using the Debye–Scherrer equation, were found to be 29.5 nm for hydrothermally synthesized MgO (HY-MgO), 33.8 nm for sol–gel-derived MgO, 49.5 nm for microwave-assisted MgO, and 44.7 nm for green-synthesized MgO nanoparticles.

The surface morphology of the synthesized MgO nanostructures was analyzed using scanning electron microscopy (SEM), as shown in Figure 4. The SEM images, especially of HY-MgO NPs, correlate well with the high-intensity peaks and crystalline features observed in the XRD patterns. Green-synthesized MgO NPs

(Figures 4a and 4b) showed uniform, spherical particles with an average size of 85.8 nm. Microwave-assisted synthesis (Figures 4c and 4d) produced irregular spherical particles around 100 nm in size. The sol–gel method (Figures 4e and 4f) resulted in uniformly distributed platelike structures with a size of approximately 70 nm. Hydrothermally synthesized MgO NPs exhibited a distinct flowerlike morphology with particles averaging 60 nm. Detailed examination revealed disc-shaped, dense, porous, and agglomerated structures. These differences in morphology among the various synthesis methods can be attributed to variations in surface energy and particle size. Elemental analysis via energy-dispersive X-ray spectroscopy (EDAX), presented in Figures 5A–D, confirmed the presence of magnesium and oxygen in all samples.

The antibacterial properties of the synthesized MgO nanostructures were evaluated using several analytical techniques. Among all the samples, the hydrothermally synthesized MgO NPs displayed the highest antibacterial activity. The zone of inhibition (ZOI) was measured using the well diffusion method, as detailed in Table 2. At a concentration of 50 mg/mL, HY-MgO NPs exhibited maximum inhibition zones of 3 mm for *Staphylococcus aureus*, 7 mm for *Enterococcus faecalis*, 5 mm for *Escherichia coli*, and 6 mm for *Klebsiella pneumoniae*. Compared to HY-MgO NPs, the antibacterial activity of MgO NPs synthesized by other methods was significantly lower, as illustrated in Figure 6.

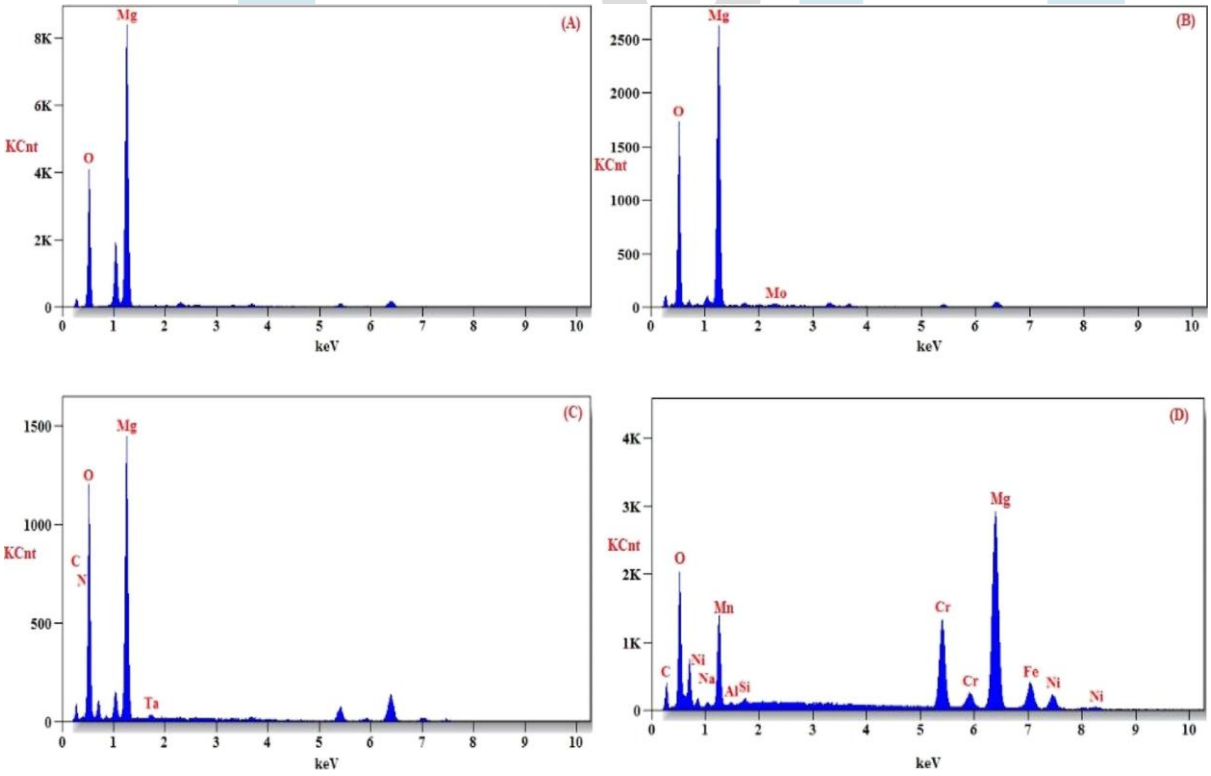

Figure 4. (A−D) EDAX micrographs of green (A), microwave (B), sol−gel (C), and hydrothermal (D) methods of preparation of MgO nanostructures.

Table 2. Zone of Inhibition of G-, M-, S-, and H-MgO NPs Activity Against *S. aureus*, *E. faecalis*, *E. coli*, and *K. pneumoniae* (A: Antibiotic Used)[a]

		ZOI (mm)																			
		green synthesis (mg/mL)					microwave synthesis (mg/mL)					sol−gel synthesis (mg/mL)					hydrothermal synthesis (mg/mL)				
s. no	name of pathogens	A	10	20	30	50	A	10	20	30	50	A	10	20	30	50	A	10	20	30	50
	E. faecalis	3	0	0	1	2	10	0	0	1.4	5.3	10.2	0	0	0	1	10.8	3	4	5	7

Numerous studies have demonstrated that the antibacterial activity of MgO nanostructures is highly dependent on particle size[18]. Huang et al. (2005) reported that reducing the particle size of MgO significantly enhanced its antibacterial properties. Specifically, within the size range of 29.5 to 49.5 nm, a gradual decrease in particle size was associated with improved bactericidal efficiency. Similarly, Makhluf et al. (2005) found that MgO nanoparticles were effective against both Gram-positive and Gram-negative bacteria, confirming a pronounced size-dependent effect—smaller particles exhibited stronger antimicrobial activity due to increased bacterial cell destruction.

This enhanced activity can be attributed to the increase in specific surface area as particle size decreases, which in turn exposes a greater number of reactive surface groups known to contribute to antibacterial effects. Among the various synthesis methods, MgO nanoparticles produced via the hydrothermal route showed the smallest average particle size (29.5 nm), thereby exhibiting superior antibacterial performance. The increased surface area provides more reactive sites, enhancing the interaction between nanoparticles and bacterial cells. This observation is also supported by Jin and He (2011), who concluded that higher concentrations of MgO nanoparticles led to increased bacterial inactivation[16].

Although the precise mechanism of bacterial inhibition by MgO nanostructures remains under investigation, several plausible pathways have been proposed[6]. These include the generation of reactive oxygen species (ROS), direct interaction of nanoparticles with bacterial cells leading to structural damage, and the induction of an alkaline environment. One widely accepted mechanism involves oxidative stress triggered by ROS production, which disrupts the integrity of bacterial cell membranes. Studies have identified superoxide anions (O_2^-) as a major ROS involved in this process. It has been shown that as the surface area of MgO nanoparticles increases, the generation of O_2^- also rises, ultimately resulting in bacterial cell death. Additionally, electrostatic interactions between the positively charged MgO nanoparticles and the negatively charged bacterial cell membranes are believed to further contribute to the antibacterial effect.

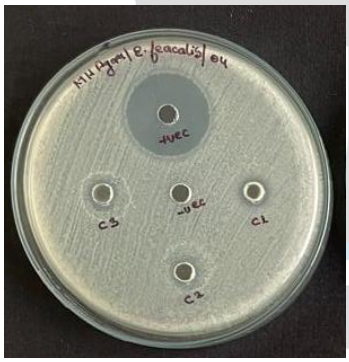

A

B

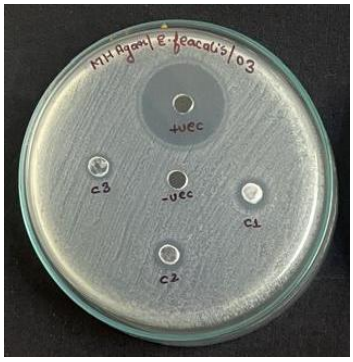

C

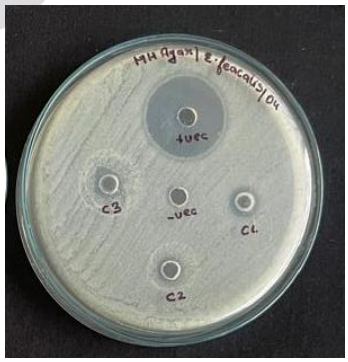

D

E F

Figure 6. ZOI of green (A & B), microwave (C&D), and sol-gel synthesized MgO NPs (E&F) activity against *E. faecalis*.

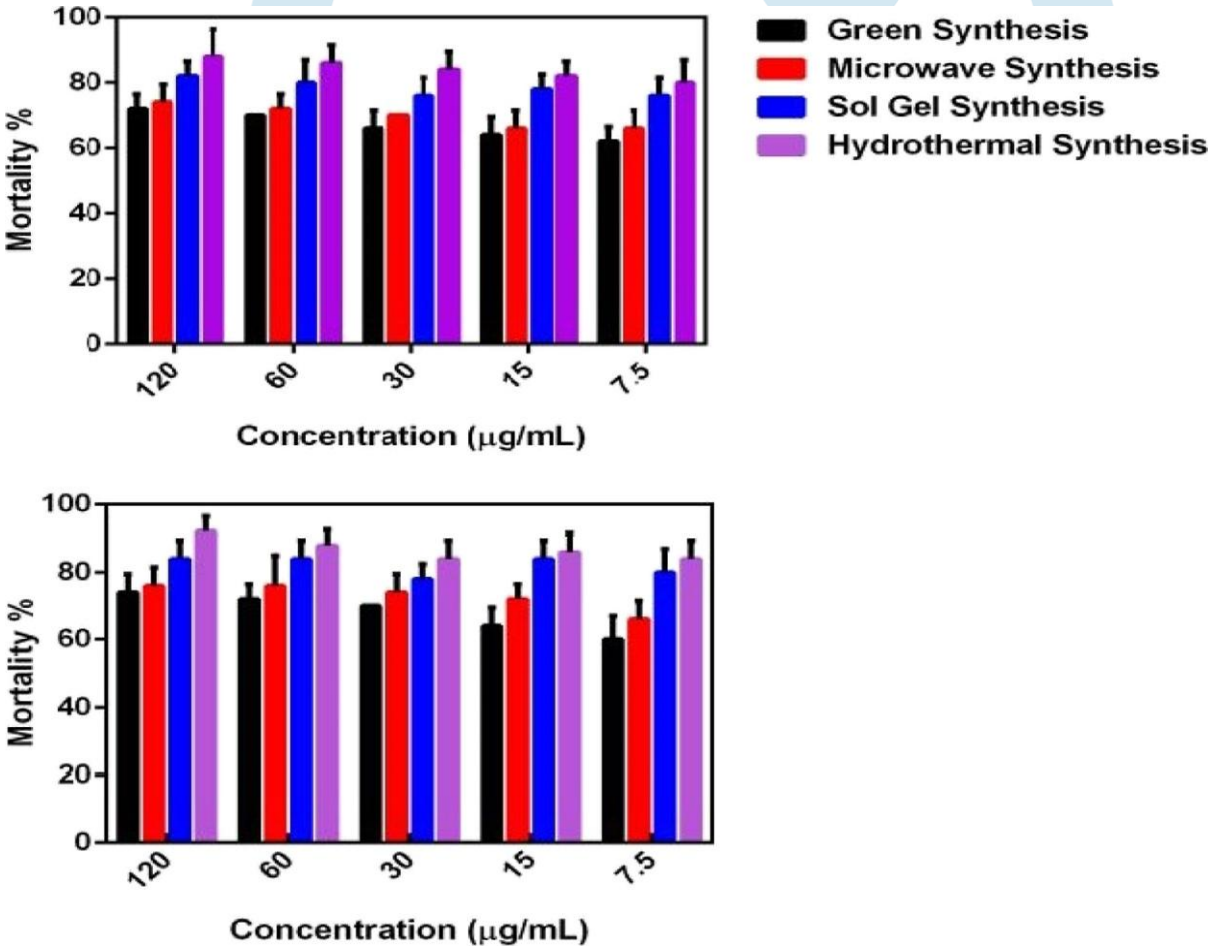

Figure 7. Mortality rate of *E. faecalis* and *E. Coli* against various concentrations of MgO NPs.

Conventional methods—both biological and chemical—have long been employed to control Bacterial diseases. However, these approaches often come with drawbacks such as toxicity to non-target organisms, including humans, and the growing resistance of bacteria to these agents[4]. In recent years, nanoparticles (NPs) have emerged as a promising alternative due to their unique physicochemical properties, offering a more effective strategy to combat bacterial-borne diseases[14].

The bactericidal efficiency of MgO nanoparticles is concentration-dependent. As illustrated in Figure 7, the mortality rates of *E. ficalis* and *E. coli* larvae vary with different concentrations of MgO NPs. The lowest mortality rate (60%) was recorded using green-synthesized MgO NPs at a concentration of 7.5 µg/mL, while the highest mortality rate (96%) was achieved with hydrothermally synthesized MgO NPs at 120 µg/mL. Notably, MgO NPs synthesized via the hydrothermal method demonstrated superior Bactericidal activity against both bacterial species compared to other synthesis techniques.

This enhanced performance can be attributed to the smaller particle size (29.5 nm) and larger surface area of hydrothermally synthesized MgO NPs, which are particularly advantageous for biomedical and entomological applications. Scanning electron microscopy (SEM) further supports this, revealing the effective interaction of these small-sized nanoparticles with pathogenic bacterial strains.

It is suggested that the reduced particle size enables MgO NPs to attach bacteria, leading to cell death. The enhanced bactericidal activity observed in hydrothermal MgO NPs may also be due to their distinct crystalline and platelike morphology, as confirmed by both XRD and FESEM analyses. Table 2 presents the LC_{50} and LC_{90} values (concentrations required to achieve 50% and 90% mortality, respectively) for MgO NPs synthesized via different methods. The results clearly show a direct correlation between nanoparticle concentration and larval mortality—higher concentrations result in increased mortality rates.

The bactericidal mechanism of MgO NPs is believed to involve several biochemical pathways, including the generation of reactive oxygen species (ROS), lipid peroxidation, and disruption of the cell membrane, leading to the leakage of intracellular components.[50],[51] Upon application to various bacteria, MgO NPs degrade into Mg^{2+} and O_2^- ions. The release of O_2^- ions promotes ROS production, which induces oxidative stress and damages cellular structures.[52] Additionally, the nanoparticles' small size enables them to interact directly with nucleic acids, disrupting genetic material and hindering mosquito development.[53] High concentrations of Mg^{2+} can further destabilize cellular equilibrium, exacerbating stress responses and leading to cell death.[54]

This study specifically investigates the bactericidal efficacy of MgO nanoparticles against *E. faecalis* and *E. coli*, highlighting the potential of nanotechnology-based strategies for disease control.

SOD

Table 3 : The activity of SOD

S.No.	Tube code	O.D at 600nm	% SOD	SOD Unit	Total SOD Unit	units/mg Fresh weight
1	Control	0.742	38.321	0.766	7.664	0.255
2	Green synthesis	0.665	44.722	0.894	8.944	0.298
3	Microwave irradiation	0.502	58.271	1.165	11.654	0.388
4	Sol–gel method	0.472	60.765	1.215	12.153	0.405
	Blank	1.203	0	0	0	0

These processes generate significant ROS, and the increased SOD activity is necessary to protect from oxidative damage. The relatively narrow range of SOD (0.405 U/ml to 0.410 U/ml) suggests that the plant has adapted to this high metabolic activity by maintaining a constant level of antioxidant defence.

Catalase

Table 3 : The activity of Catalase

S.No.	Tube code	O.D. at 240nm	Concentration of H_2O_2 (nM min^{-1})
1	Control	0.0821	2.08
2	IN I	0.0659	1.67
3	IN II	0.098	2.48
4	SA I	0.056	1.42
5	SA II	0.051	1.29

In this study catalase (CAT) activity, an important antioxidant enzyme responsible for the breakdown of hydrogen peroxide into water and oxygen, has been quantitatively assessed to evaluate the plant's oxidative stress management capability under in vitro conditions. In internode cultures of *Mucuna pruriens*, catalase activity was observed in the range of 8.35 nM min^{-1}/g – 12.4 nM min^{-1}/g. This elevated level suggests a relatively robust antioxidative defence mechanism.

CONCLUSIONS

MgO nanostructures were successfully synthesized using four distinct methods. The resulting nanoparticles were thoroughly characterized using X-ray diffraction (XRD), Fourier-transform infrared spectroscopy (FT-IR), and scanning electron microscopy with energy-dispersive X-ray analysis (SEM-EDAX). Among the synthesized samples, hydrothermal MgO nanoparticles exhibited superior morphology with the smallest particle size of 29.5 nm. SEM imaging revealed various structural morphologies: green-synthesized MgO NPs displayed a uniform spherical shape, microwave-assisted NPs showed an irregular spherical pattern, sol–gel-synthesized NPs formed uniform plate-like structures, and hydrothermal NPs featured a distinctive flower-like morphology.

The antibacterial efficacy of these nanostructures was assessed against pathogenic bacterial strains including *Enterococcus faecalis* and *Escherichia coli*. Results confirmed that antibacterial activity is concentration-dependent. Notably, hydrothermally synthesized MgO NPs at a concentration of 50 mg/mL demonstrated significant inhibitory zones of 7 mm for *E. faecalis*. For *E. coli*, the highest zone of inhibition (9 mm) was recorded using sol–gel-synthesized MgO NPs at the same concentration.

REFERENCES

1. Baptista, P. V., McCusker, M. P., Carvalho, A., Ferreira, D. A., Mohan, N. M., Martins, M., & Fernandes, A. R. (2018). Nano-strategies to fight multidrug resistant bacteria—"A Battle of the Titans." *Frontiers in Microbiology*, *9*, 1441.
2. Nadeem, S. F., Gohar, U. F., Tahir, S. F., Mukhtar, H., Pornpukdeewattana, S., Nukthamna, P., Moula Ali, A. M., Bavisetty, S. C. B., & Massa, S. (2020). Antimicrobial resistance: More than 70 years of war between humans and bacteria. *Critical Reviews in Microbiology*, *46*(5), 578–599.
3. Hollyer, I., & Ison, M. G. (2018). The challenge of urinary tract infections in renal transplant recipients. *Transplant Infectious Disease*, *20*(2), e12828. https://doi.org/10.1111/tid.12828
4. Metwaly, A. M., Ghoneim, M. M., Eissa, I. H., Elsehemy, I. A., Mostafa, A. E., Hegazy, M. M., Afifi, W. M., & Dou, D. (2021). Traditional ancient Egyptian medicine: A review. *Saudi journal of biological sciences*, *28*(10), 5823–5832.
5. Muhammad H, Muhammad S (2005) The use of Lawsonia inermis Linn.(henna) in the management of burn wound infections. African Journal of Biotechnology 4 (9)
6. Avci, H., Monticello, R., & Kotek, R. (2013). Preparation of antibacterial PVA and PEO nanofibers containing Lawsonia Inermis (henna) leaf extracts. *Journal of Biomaterials Science, Polymer Edition*,

24(16), 1815–1830. https://doi.org/10.1080/09205063.2013.804758

7. Singh, D. K., Luqman, S., & Mathur, A. K. (2015). Lawsonia inermis L. – A commercially important primaeval dying and medicinal plant with diverse pharmacological activity: A review. *Industrial Crops and Products, 65*, 269–286. https://doi.org/10.1016/j.indcrop.2014.11.025
8. Barani, M., Mirzaei, M., Torkzadeh-Mahani, M., & Nematollahi, M. H. (2018). Lawsone-loaded Niosome and its antitumor activity in MCF-7 breast cancer cell line: A nano-herbal treatment for cancer. *DARU Journal of Pharmaceutical Sciences, 26*(1), 11–17. https://doi.org/10.1007/s40199-018-0207-3
9. Rehman, F.-u, Adeel, S., Qaiser, S., Bhatti, I. A., Shahid, M., & Zuber, M. (2012). Dyeing behaviour of gamma irradiated cotton fabric using Lawson dye extracted from henna leaves (Lawsonia inermis). *Radiation Physics and Chemistry, 81*(11), 1752–1756.
10. Khan, B. A., Khan, A., Khan, M. K., & Braga, V. A. (2021). Preparation and properties of high sheared poly (vinyl alcohol)/chitosan blended hydrogels films with Lawsonia inermis extract as wound dressing. *Journal of Drug Delivery Science and Technology, 61*, 102227.
11. Hsouna, A. B., Trigui, M., Culioli, G., Blache, Y., & Jaoua, S. (2011). Antioxidant constituents from Lawsonia inermis leaves: Isolation, structure elucidation and antioxidative capacity. *Food Chemistry, 125*(1), 193–200.
12 Salem, S. S., Hammad, E. N., Mohamed, A. A., & El-Dougdoug, W. (2023). A comprehensive review of nanomaterials: Types, synthesis, characterization, and applications. *Biointerface Research in Applied Chemistry, 13*(1), 41. https://doi.org/10.33263/BRIAC131.041
13. Salem, S. S., & Fouda, A. (2021). Green synthesis of metallic nanoparticles and their prospective biotechnological applications: An overview. *Biological Trace Element Research, 199*(1), 344–370. https://doi.org/10.1007/s12011-020-02138-3
14. AbdElkodous, M., El-Husseiny, H. M., El-Sayyad, G. S., Hashem, A. H., Doghish, A. S., Elfadil, D., Radwan, Y., El-Zeiny, H. M., Bedair, H., & Ikhdair, O. A. (2021). Recent advances in waste-recy- cled nanomaterials for biomedical applications: Waste-to-wealth. *Nanotechnology Reviews, 10*(1), 1662–1739.
15. Shehabeldine, A. M., Hashem, A. H., Wassel, A. R., & Hasanin, M. (2022). Antimicrobial and antiviral activities of durable cotton fabrics treated with nanocomposite based on zinc oxide nanoparticles, acyclovir, nanochitosan, and clove oil. *Applied Biochemistry and Biotechnology, 194*(2), 783–800. https://doi.org/10.1007/s12010-021-03649-y
16. Hasanin M, Hashem AH, Lashin I, Hassan SAM (2021) In vitro improvement and rooting of banana plantlets using antifungal nanocomposite based on myco-synthesized copper oxide nanoparticles and starch. Biomass Conversion and Biorefineryhttps://doi.org/10.1007/s13399-021-01784-4
17. Shehabeldine, A. M., Salem, S. S., Ali, O. M., Abd-Elsalam, K. A., Elkady, F. M., & Hashem, A. H. (2022). Multifunctional silver nanoparticles based on chitosan: Antibacterial, antibiofilm, antifungal, antioxidant, and wound-healing activities. *Journal of Fungi, 8*(6), 612.
18. Elbasuney, S., El-Sayyad, G. S., Tantawy, H., & Hashem, A. H. (2021). Promising antimicrobial and antibiofilm activities of reduced graphene oxide-metal oxide (RGO-NiO, RGO-AgO, and RGO-ZnO) nanocomposites. *RSC advances, 11*(42), 25961–25975.